J Eng Math (2009) 65:229–242
DOI 10.1007/s10665-009-9283-1

Effect of inertia on electrified film flow over a wavy wall

D. Tseluiko · M. G. Blyth

Received: 12 February 2008 / Accepted: 25 February 2009 / Published online: 14 March 2009

Abstract The effect of inertia on the steady flow of a liquid layer down a wavy wall in the presence of an electric field is investigated. Both the liquid film and the region above it are assumed to act as perfect dielectrics. A linearised perturbation analysis is performed for flow down a wall with small-amplitude sinusoidal corrugations, and the free-surface amplitude and phase shift are computed numerically for a broad range of flow conditions. It is shown that the electric field can be used to manipulate the phase shift between the free surface and the wall. In particular, when the Reynolds number lies below a threshold value, an electric field of sufficient strength will bring the free surface precisely into phase with the wall. An electric field can also be used to mitigate the resonance effect identified by previous workers, in which the free surface suffers significant amplification in comparison to the height of the wall corrugations at a particular Reynolds number. Working on the basis of the lubrication approximation, a nonlinear equation for the film thickness is derived featuring a non-local term due to the electric field. Numerical solutions for flow over a wavy wall of finite amplitude reveal that the effect of inertia on the free-surface characteristics depends on the electrical properties of the fluid layer and the strength of the imposed electric field.

Keywords Corrugated wall · Electrohydrodynamics · Film flow

1 Introduction

Gravity-driven flow of a liquid film down an inclined wall arises in a number of important applications including coating technologies (e.g. [1,2]), heat exchangers (e.g. [3]), and microfluidics (e.g. [4]). While theoretical studies have tended to work on the assumption of a flat wall, in practice wall irregularities may have a significant effect on the film dynamics. Natural wall imperfections may come as an unavoidable and unwelcome feature, for example in coating flow applications where usually a layer of uniform thickness is required, but in other situations they may be engineered deliberately to advantage, for example to maximise heat transport across a cooling film.

Earlier work on film flow over an uneven wall has shown that the flow structure is highly sensitive to the wall geometry. Wang [5] carried out an asymptotic study of film flow down a wall with small-amplitude corrugations at zero Reynolds number and found that in general there is a phase shift between the free surface and the wall

D. Tseluiko · M. G. Blyth (✉)
School of Mathematics, University of East Anglia, Norwich, NR4 7TJ, UK
e-mail: m.blyth@uea.ac.uk

whose magnitude depends on the parameter values. Tougou [6] performed a weakly nonlinear analysis and developed equations describing the film thickness when the wall geometry varies slowly in the streamwise direction. In later work, Wang [7] relaxed the assumption of small-amplitude corrugations and developed a thin-film theory for flow along a curved surface whose minimum radius of curvature is much larger than the film thickness. A critical assessment of Wang's work including some experimental results can be found in [8]. Pozrikidis [9] carried out an analysis of film flow down a periodic wall of small amplitude in the presence of an insoluble surfactant and performed boundary-element computations for finite-amplitude walls. Film flow over a wall with large amplitude corrugations was also discussed in the context of Stokes flow by Wierschem et al. [10] and Scholle et al. [11], and in the presence of inertia by Wierschem and Aksel [12]. Further numerical studies of falling film flow include those by Malamataris and Bontozoglou [13], Trifonov [14], and Gu et al. [15], who considered flow over an uneven wall at arbitrary Reynolds number. Recently, Luo and Pozrikidis [16] considered shear-driven flow of two superposed layers in a channel with a periodic wall at zero Reynolds number and described the effect of an insoluble surfactant at the interface. Their work was extended to the case of arbitrary Reynolds number by Luo et al. [17]. The effect of inertia on film flow over localised topography has been investigated by Gaskell et al. [18] and by Saprykin et al. [19].

In this paper, we study the effect of inertia on film flow over a wavy wall in the presence of an electric field. Our work complements the recent study by Tseluiko et al. [20], who examined electrified film flow at zero Reynolds number over sinusoidal and indented walls. They showed that the electric field can be used to control the amplitude of the free-surface wave and its phase shift relative to the wall profile. In the present work, we extend the previous results to the case of finite Reynolds number and study the role played by inertia in determining the shape of the free surface under steady conditions. We begin by performing a linearised analysis on the assumption of a small-amplitude sinusoidal wall and compute the amplitude and phase shift of the free-surface deformation wave. Results for film flow over wavy walls of arbitrary amplitude are computed using a long-wave model that generalises Tseluiko and Papageorgiou's [21] work for a perfect-conductor film on a flat wall to the case when the film is treated as a perfect dielectric. The perfect-conductor case is retrieved in the limit of infinite relative permittivity.

In Sect. 2 we describe the physical problem and present the governing equations. In Sect. 3 we conduct an asymptotic analysis and present results for a small-amplitude sinusoidal wall. In Sect. 4 we perform a long-wave asymptotic analysis for wall corrugations of finite amplitude and derive a nonlinear long-wave equation for the film thickness which we solve numerically. In Sect. 5 we present our conclusions.

2 Problem formulation

We consider the steady, gravity-driven flow of a liquid film down a wavy wall which is inclined at an angle β to the horizontal, as is illustrated in Fig. 1. Referring to the Cartesian coordinates $(x,\ z)$ shown in the figure, the wall is located at $z = s(x)$, where s is a given function, and the film surface is located at $z = f(x)$, where f is to be found. The film is subjected to an electric field which acts in the positive z-direction with strength E_0 sufficiently far from the film. The wall is treated as an equipotential surface held at zero voltage. The liquid is assumed to be a perfect dielectric of permittivity ε_1, and the air above the film is assumed to be a perfect dielectric of permittivity ε_2. The relative permittivity is $\varepsilon_p \equiv \varepsilon_1/\varepsilon_2$. In the limit $\varepsilon_p \to \infty$, the film behaves as a perfect conductor and the electric field inside the film vanishes (e.g. [22]).

The velocity and pressure fields in the film are given by $\mathbf{u} = (u,\ v)$ and p, respectively. The electric potentials, $\varphi_j(x,\ z)$, and electric fields, $\mathbf{E}_j$, satisfy the relations $\mathbf{E}_j = -\nabla\varphi_j$, where $j = 1$ corresponds to the liquid and $j = 2$ corresponds to the air. Using an asterisk to denote a dimensionless quantity, we non-dimensionalise variables by writing

$$\begin{aligned} &x^* = \frac{1}{h_0}x, \quad z^* = \frac{1}{h_0}z, \quad f^* = \frac{1}{h_0}f, \quad s^* = \frac{1}{h_0}s, \\ &u^* = \frac{1}{U_0}u, \quad v^* = \frac{1}{U_0}v, \quad p^* = \frac{h_0}{\mu U_0}p, \quad \varphi_{1,2}^* = \frac{1}{E_0 h_0}\varphi_{1,2}, \end{aligned} \tag{1}$$

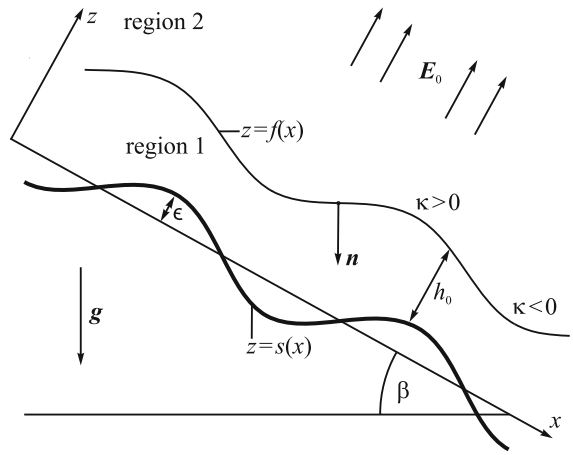

Fig. 1 Schematic of the problem: gravity-driven flow of a liquid film down a wavy wall in the presence of an electric field

where h_0 is the average film thickness, $U_0 = \rho g h_0^2 \sin\beta/2\mu$ is the Nusselt surface speed of a flat film flowing down an inclined plane, ρ and μ are the density and viscosity of the fluid respectively and g is gravity. Henceforth we drop the asterisk superscripts and deal only with dimensionless quantities.

The flow in the liquid film is governed by the Navier–Stokes and continuity equations,

$$R(\mathbf{u}\cdot\nabla\mathbf{u}) = -\nabla p + \mathbf{G} + \nabla^2\mathbf{u}, \quad \nabla\cdot\mathbf{u} = 0, \tag{2}$$

where $\mathbf{G} = (2,\ -2\cot\beta)$ and R is the Reynolds number defined below. The no-slip and no-penetration conditions require that $\mathbf{u} = \mathbf{0}$ at the wall, $z = s(x)$. The kinematic condition at the film surface, $z = f(x)$, requires that $\mathbf{u}\cdot\mathbf{n} = 0$, where $\mathbf{n}$ is the unit normal to the film surface pointing into the film. The dynamic stress balance at the free surface demands that

$$\boldsymbol{\sigma}_1\cdot\mathbf{n} = -(\kappa/C + P_a)\,\mathbf{n} + (\mathbf{M}_2 - \mathbf{M}_1)\cdot\mathbf{n} \tag{3}$$

at $z = f(x)$, where κ is the free-surface curvature taken to be positive when the surface is concave downwards as shown in Fig. 1, C is the capillary number defined below, P_a is a constant reference pressure, and $\boldsymbol{\sigma}_1$ is the Newtonian stress tensor in the liquid. The Maxwell stress tensors in the liquid and in the air are given by (e.g. [23]) $\mathbf{M}_1 = \varepsilon_p W_e\left(\mathbf{E}_1\mathbf{E}_1 - \mathbf{I}|\mathbf{E}_1|^2/2\right)$ and $\mathbf{M}_2 = W_e\left(\mathbf{E}_2\mathbf{E}_2 - \mathbf{I}|\mathbf{E}_2|^2/2\right)$, where W_e is the electric Weber number defined below.

The electric potentials, φ_1 and φ_2, satisfy Laplace's equation

$$\nabla^2\varphi_j = 0 \tag{4}$$

in the film ($j = 1$) and in the air ($j = 2$). At the wall, $z = s(x)$, the potential is taken to be zero, $\varphi_1 = 0$. In the far field, we have $\nabla\varphi_2 \to -\mathbf{k}$ as $z \to \infty$, where $\mathbf{k}$ is a unit vector pointing in the positive z-direction, corresponding to the uniform-electric-field condition at infinity. At the free surface, $z = f(x)$, the conditions of continuity of the electric potential and continuity of the normal component of the electric displacement are (e.g. [24, p. 16])

$$\varphi_1 = \varphi_2, \quad \varepsilon_p(\mathbf{n}\cdot\nabla\varphi_1) = \mathbf{n}\cdot\nabla\varphi_2. \tag{5}$$

The film dynamics depends upon the values of the Reynolds number, R, the capillary number, C, and the electric Weber number, W_e, which are defined as

$$R = \frac{\rho h_0 U_0}{\mu} = \frac{\rho^2 g h_0^3 \sin\beta}{2\mu^2}, \quad C = \frac{\mu U_0}{\gamma} = \frac{\rho g h_0^2 \sin\beta}{2\gamma}, \quad W_e = \frac{\varepsilon_2 E_0^2 h_0}{2\mu U_0} = \frac{\varepsilon_2 E_0^2}{\rho g h_0 \sin\beta}, \tag{6}$$

where γ is the surface tension.

3 Flow over a wall with small-amplitude sinusoidal corrugations

In this section, we perform a linearised analysis of the flow of a liquid film down a wall with sinusoidal corrugations of dimensionless period L and small amplitude ϵ, where $\epsilon \ll 1$. The wall shape is given by

$$s(x) = \epsilon\, \mathrm{e}^{\mathrm{i}kx}, \tag{7}$$

where $k = 2\pi/L$ is the wavenumber of the corrugations, and the real part of the right-hand side is to be understood. Since the flow is assumed to be two-dimensional, it is convenient to introduce a stream function, $\psi(x,\, z)$, defined in the usual way so that $u = \partial\psi/\partial z$ and $v = -\partial\psi/\partial x$.

In the unperturbed state, when $\epsilon = 0$, the free surface is perfectly flat, $f \equiv 1$, and the flow is represented by the classical Nusselt profile,

$$\psi_0 = z^2 - \frac{z^3}{3}. \tag{8}$$

The unperturbed pressure field is given by

$$p_0 = P_a - 2(z-1)\cot\beta\, - \left(1 - \frac{1}{\varepsilon_p}\right) W_e, \tag{9}$$

and the unperturbed electric potentials are given by

$$\varphi_{10} = -\frac{1}{\varepsilon_p} z, \quad \varphi_{20} = -z + 1 - \frac{1}{\varepsilon_p}. \tag{10}$$

For the corrugated wall, we perturb the free-surface shape by writing

$$f = 1 + \epsilon\, A_1\, \mathrm{e}^{\mathrm{i}kx} + \cdots, \tag{11}$$

where A_1 is a constant to be found, and expand the flow variables as follows,

$$\psi = \psi_0 + \epsilon\, \psi_1(z)\, \mathrm{e}^{\mathrm{i}kx} + \cdots, \quad p = p_0 + \epsilon\, p_1(z)\, \mathrm{e}^{\mathrm{i}kx} + \cdots. \tag{12}$$

Similarly, we expand the electric potentials by writing

$$\varphi_j = \varphi_{j0} + \epsilon\, \varphi_{j1}(z)\, \mathrm{e}^{\mathrm{i}kx} + \cdots, \tag{13}$$

for $j = 1,\, 2$.

For the electric field problem, substituting (13) in (4) and the corresponding boundary conditions, we obtain

$$\varphi_{j1}'' - k^2 \varphi_{j1} = 0 \tag{14}$$

for $j = 1,\, 2$ together with $\varphi_{11}(0) = 1/\varepsilon_p$, $\varphi_{21}(1) - \varphi_{11}(1) = (1 - 1/\varepsilon_p)A_1$, $\varepsilon_p \varphi_{11}'(1) = \varphi_{21}'(1)$, and $\varphi_{21} \to 0$, $\varphi_{21}' \to 0$ as $z \to \infty$. The solutions are

$$\varphi_{11} = \frac{\cosh\big[k(z-1)\big] - (1/\varepsilon_p)\sinh\big[k(z-1)\big] - (1 - 1/\varepsilon_p)A_1 \sinh kz}{\varepsilon_p \cosh k + \sinh k}, \tag{15}$$

$$\varphi_{21} = \frac{\big[1 - (1-\varepsilon_p)A_1 \cosh k\big]\mathrm{e}^{-k(z-1)}}{\varepsilon_p \cosh k + \sinh k}. \tag{16}$$

For the fluid problem, substituting (12) in (2) and eliminating the pressure yields the governing equation

$$\psi_1'''' - 2k^2\, \psi_1'' + k^4\, \psi_1 = \mathrm{i}kR\left[(2z - z^2)\big(\psi_1'' - k^2\psi_1\big) + 2\psi_1\right]. \tag{17}$$

The no-slip and no-penetration conditions imply

$$\psi_1(0) = 0, \quad \psi_1'(0) = -2. \tag{18}$$

The kinematic condition gives

$$\psi_1(1) = -A_1, \tag{19}$$

and the tangential and normal stress balances require

$$\psi_1''(1) + k^2\psi_1(1) = 2A_1, \quad \psi_1'''(1) - (3k^2 + \mathrm{i}kR)\psi_1'(1) = 2\mathrm{i}k\big(\tau A_1 - \sigma\big), \tag{20}$$

respectively, where we have made use of the electric field solutions (15) and (16). It should be noted that the electric field only makes a contribution to the normal component of the stress balance. Here,

$$\tau = \frac{1}{2C}k^2 - \left(1 - \frac{1}{\varepsilon_p}\right)^2 W_e \frac{k}{1 + (1/\varepsilon_p)\tanh k} + \cot\beta, \tag{21}$$

$$\sigma = \left(\frac{1}{\varepsilon_p} - \frac{1}{\varepsilon_p^2}\right) W_e \frac{k}{\cosh k + (1/\varepsilon_p)\sinh k}. \tag{22}$$

When the liquid behaves as a perfect conductor, these simplify to

$$\tau = \frac{1}{2C}k^2 - W_e k + \cot\beta, \quad \sigma \equiv 0, \tag{23}$$

on taking the limit $\varepsilon_p \to \infty$.

In general, the problem is to find A_1 by solving (17) subject to (18)–(20) for a particular choice of the wall wavenumber k, the inclination angle, β, and the dimensionless parameters R, C, and W_e. At zero Reynolds number, $R = 0$, the solution for arbitrary wavenumber k was obtained by Tseluiko et al. [20], who showed that

$$A_1 = \frac{2k^2\cosh k - \mathrm{i}(\cosh k \sinh k - k)\sigma}{k^2 + k^4 + k^2\cosh^2 k - \mathrm{i}(\cosh k \sinh k - k)\tau}. \tag{24}$$

At finite Reynolds number, the problem for arbitrary wavenumber must be solved numerically, as will be done below. Some analytical progress can be made in the limit of small wavenumber, $k \to 0$, as will be discussed next.

3.1 Long-wave approximation

We work on the assumption that the dimensionless wavelength, L, of the sinusoidal wall is large, so that the wavenumber $k = 2\pi/L \ll 1$, and seek a solution by expanding ψ_1 and A_1 in power series in k, writing

$$\psi_1 = \psi_1^{(0)} + k\,\psi_1^{(1)} + k^2\,\psi_1^{(2)} + \cdots, \quad A_1 = A_1^{(0)} + k\,A_1^{(1)} + k^2\,A_1^{(2)} + \cdots. \tag{25}$$

Keeping the first m terms in the expansions (25), asymptotic consistency is maintained provided that $k \gg \epsilon^{1/m}$, in which case all of the retained m terms enter (11) and (12) at an order lower than $O(\epsilon^2)$.

We will consider two cases. In the first case, we assume that $C = O(k^3)$ and $W_e = O(k^{-2})$. These were the scalings adopted by Tseluiko et al. [22] in their study of electrified flow over topography. In the second case, we assume that $C = O(k^2)$ and $W_e = O(k^{-1})$, corresponding to the scalings adopted by Tseluiko and Papageorgiou [21] in their analysis of electrified flow down an inclined plane. For the first set of scalings, both capillary and electric effects enter at leading order, whereas for the second set of scalings capillary and electric effects enter at first order.

3.1.1 The case $C = O(k^3)$ and $W_e = O(k^{-2})$

To analyse this case, we write $C = k^3 C'$ and $W_e = W_e'/k^2$, where both C' and W_e' are $O(1)$ parameters. The remaining parameters R, $\cot\beta$, and $1/\varepsilon_p$ are all assumed to be of $O(1)$. Substituting expansions (25) in (17)–(20), at leading order we obtain a linear problem for $\psi_1^{(0)}$ which has a solution if and only if

$$A_1^{(0)} = \frac{3 - \mathrm{i}\hat{\sigma}_0}{3 - \mathrm{i}\hat{\tau}_0}, \tag{26}$$

where

$$\hat{\tau}_0 = \frac{1}{2C'} - \frac{(1-\varepsilon_p)^2}{\varepsilon_p^2} W_e', \quad \hat{\sigma}_0 = \frac{\varepsilon_p - 1}{\varepsilon_p^2} W_e'. \tag{27}$$

If this condition is satisfied, the solution for $\psi_1^{(0)}$ is a cubic polynomial in z. The problem at first order for $\psi_1^{(1)}$ has a solution if and only if

$$A_1^{(1)} = \frac{\left(\mathrm{i}\hat{\tau}_1 + 3\mathrm{i}R\left[\frac{3}{20} - \frac{37}{420}\mathrm{i}\hat{\tau}_0\right]\right) A_1^{(0)} - \mathrm{i}\hat{\sigma}_1 - 3\mathrm{i}R\left(\frac{3}{20} - \frac{37}{420}\mathrm{i}\hat{\sigma}_0\right)}{3 - \mathrm{i}\hat{\tau}_0}, \tag{28}$$

where

$$\hat{\tau}_1 = \frac{(1-\varepsilon_p)^2}{\varepsilon_p^3} W_e' + \cot\beta, \quad \hat{\sigma}_1 = \frac{1-\varepsilon_p}{\varepsilon_p^3} W_e'. \tag{29}$$

Provided this condition is satisfied, the solution for $\psi_1^{(1)}$ is a seventh-order polynomial in z. It will be noted that the Reynolds number, and hence the effect of inertia, enters the solution only at first order.

3.1.2 The case $C = O(k^2)$ and $W_e = O(k^{-1})$

To study this case, we let $C = k^2\,\overline{C}$ and $W_e = \overline{W}_e/k$, where both $\overline{C}$ and $\overline{W}_e$ are $O(1)$ parameters. The remaining parameters R, $\cot\beta$, and $1/\varepsilon_p$ are assumed to all be of $O(1)$. Proceeding as in Sect. 3.1.1, we find that the Reynolds number now enters the problem at second order. Specifically, we derive the following expression for the relative complex amplitude correct to $O(k^3)$,

$$A_1 = 1 + \frac{\mathrm{i}}{3}(\tau_0 - \sigma_0)\,k + \left(-\frac{1}{2} - \frac{1}{9}\tau_0(\tau_0 - \sigma_0) + \frac{4R}{105}(\tau_0 - \sigma_0) + \frac{\mathrm{i}}{3}(\tau_1 - \sigma_1)\right) k^2, \tag{30}$$

where

$$\tau_0 = \frac{1}{2\overline{C}} - \frac{(1-\varepsilon_p)^2}{\varepsilon_p^2}\overline{W}_e + \cot\beta, \quad \sigma_0 = \frac{\varepsilon_p - 1}{\varepsilon_p^2}\,\overline{W}_e, \tag{31}$$

and

$$\tau_1 = \frac{(1-\varepsilon_p)^2}{\varepsilon_p^3}\,\overline{W}_e, \quad \sigma_1 = \frac{1-\varepsilon_p}{\varepsilon_p^3}\,\overline{W}_e. \tag{32}$$

By expanding for small k and setting $R = 0$, it may be verified directly that expressions (26), (28) and (30) are consistent with the solution for Stokes flow (24).

3.2 Numerical method and results

For general wavenumber, the problem for A_1 must be solved numerically. We follow the Chebyshev tau approach utilised by Luo et al. [17] in their study of two-layer flow in a channel with a wavy wall, and expand the stream function in a series of Chebyshev polynomials, T_n. First, using the transformation $y = 2z - 1$, we map the flow domain $z \in [0,\ 1]$ onto the canonical domain of definition for Chebyshev functions, $y \in [-1,\ 1]$. Next, we expand the stream function as a series of Chebyshev polynomials, writing

$$\psi_1(y) = \sum_{n=0}^{N} a_n\,T_n(y), \tag{33}$$

where N is a specified truncation level and a_n are constant coefficients to be determined. Substituting (33) in (17) and projecting the resulting equation onto $T_m(y)$ for $m = 0, \ldots, N-3$ under the Chebyshev inner product,

$$\langle T_m(y),\ f(y)\rangle = \int_{-1}^{1} \frac{1}{\sqrt{1-y^2}}\,T_m(y) f(y)\,\mathrm{d}y, \tag{34}$$

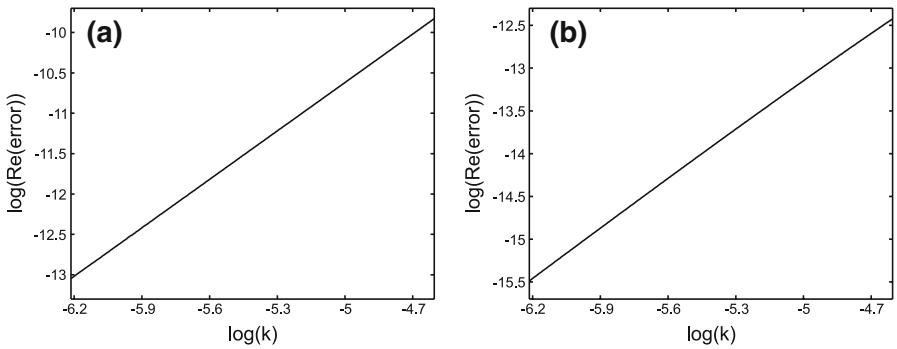

Fig. 2 The variation with k of the absolute values of (**a**) the real and (**b**) the imaginary parts of the difference between the numerically computed value of A_1 and the asymptotic result obtained in Sect. 3.1.1 for the case $C' = 1$, $W_e' = 1$, $\varepsilon_p = 3$, $R = 5$, and $\beta = 30°$. The results are presented on a log–log scale

we obtain a set of $N - 3$ algebraic equations. Five more equations follow by substituting (33) in the boundary conditions (18)–(20) to complete a set of $N + 2$ linear equations for the $N + 1$ unknown coefficients a_n and the unknown relative complex amplitude, A_1. The system of linear equations is solved using Gaussian elimination. In practice, fixing the truncation level up to $N = 50$ produces accurate results for different choices of the parameter values.

To validate the code, we checked the numerically computed values of A_1 against the asymptotic results for walls of large wavelength obtained in Sects. 3.1.1 and 3.1.2. Figure 2 displays the real and imaginary parts of the error for small values of k for the case $C' = 1$, $W_e' = 1$, $\varepsilon_p = 3$, $R = 5$, and $\beta = 30°$ on a log–log scale. The error is defined to be the absolute difference between the numerically computed value of A_1 and the asymptotic prediction $A_1^{(0)} + \epsilon\, A_1^{(1)}$, where $A_1^{(0)}$ and $A_1^{(1)}$ are given by (26) and (28) respectively. The error decreases as k decreases. Moreover, the graphs are approximately straight lines of slope 2, which is to be expected since the asymptotic result of sect. 3.1.1 is correct to $O(k^2)$.

For the remainder of this section, we fix the capillary number and the inclination angle, setting $C = 1$ and $\beta = 10°$, and study the effect of varying the Reynolds number, the electric Weber number, and the relative permittivity of the fluid film. Before presenting our results, we begin with a discussion of the likely stability of the liquid film under the parametric conditions to be considered. The film is unstable at a sufficiently large Reynolds number. Yih [25] identified the critical Reynolds number corresponding to long wavelength instability for a film falling down a flat incline. Kim et al. [26] investigated the stability of a liquid film flowing down an inclined plane in the presence of an electric field at finite Reynolds number.

In Fig. 3, we display neutral curves arising from the linear stability analysis for film flow down a plane inclined at 10° computed using the numerical method described by Blyth [27]. The thin line shows the neutral curve in the absence of an electric field, and the thick line shows the neutral curve when $W_e = 3.25$ and the film is assumed to be a perfect conductor. Regions of stability above the neutral curves are marked with an S and regions of instability below the neutral curves are marked with a U. The critical Reynolds number for instability for the non-electrified flow is $R_c = 7.09$; the critical value for the electrified flow is very slightly lower. The effect of wall corrugations is generally deemed to be stabilising. Vlachogiannis and Bontozoglou [28] conducted film flow experiments down a slightly inclined wall indented with rectangular corrugations and showed that the corrugations tend to elevate the critical Reynolds number for stability. This observation was supported theoretically by Wierschem and Aksel [29] and experimentally by Wierschem and Aksel [30] for flow down a sinusoidal wall. Vlachogiannis and Bontozoglou [28] found that a steady, deformed free surface is seen over about the first 8 wall wavelengths beyond the point of deposition of the fluid film even for Reynolds numbers well above the critical value. Moreover, they noted the importance of steady solutions in determining the dynamics of the other more complex flow regimes which emerge at larger Reynolds number. Keeping the preceding remarks in mind, in what follows we present results for Reynolds numbers which extend beyond the theoretical critical value for stability on a flat incline.

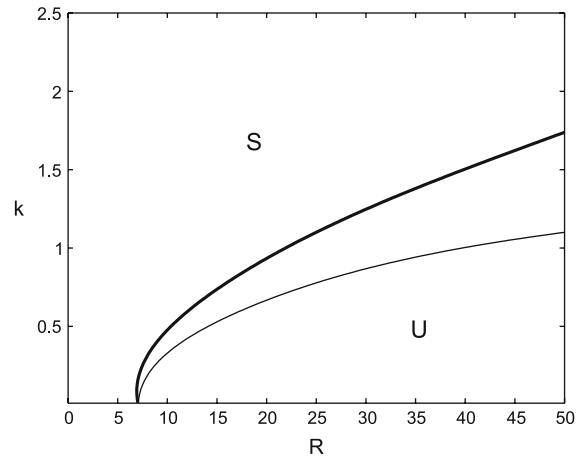

Fig. 3 The linear stability neutral curves in Reynolds number/wavenumber $(R,\ k)$ space for the case $C = 1$, $\beta = 10°$, when $W_e = 0$ (*thin line*) and $W_e = 3.25$ for a perfect-conductor film (*solid line*). Points in the regions marked U underneath the curves correspond to unstable modes and points in the regions marked S above the curves correspond to stable modes

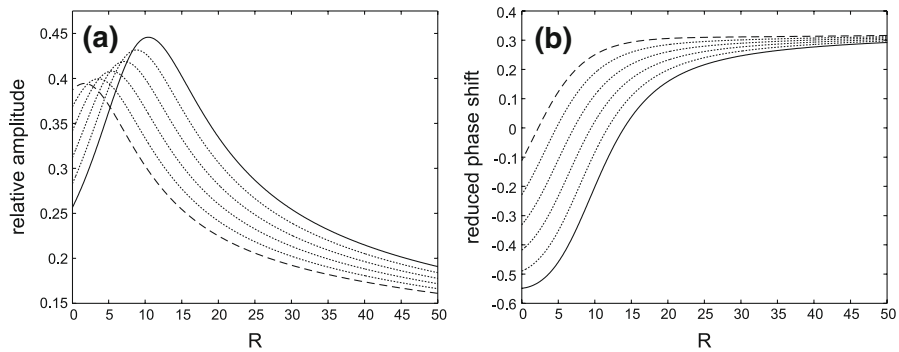

Fig. 4 The variation of (**a**) the relative amplitude, $|A_1|$, and (**b**) the reduced phase shift, $-\mathrm{Arg}(A_1)/(\pi/2)$, with the Reynolds number, R, for the case $C = 1$, $\beta = 10°$, and $k = 2$. The film is taken to be a perfect conductor and the different curves correspond to Weber numbers, W_e, that are evenly-spaced from 0 (*solid line*) to 3.25 (*dashed line*)

Figure 4(a, b) displays, respectively, the relative amplitude, $|A_1|$, and the reduced phase shift, defined as $-\mathrm{Arg}(A_1)/(\pi/2)$, against Reynolds number when $k = 2$ and the film is a perfect conductor, corresponding to $\varepsilon_p = \infty$. The different curves in Figs. 4(a, b) show results at evenly-spaced values of the Weber number, W_e, between 0, shown with a solid line, and 3.25, shown with a dashed line. For a positive/negative value of the reduced phase shift, the free-surface profile is shifted to the right/left with respect to the wall. The neutral curves shown in Fig. 3 suggest that a surface disturbance, which has the same wavenumber $k = 2$ as the wall profile, is stable over the range of Reynolds numbers shown in Fig. 4 for all W_e up to about 3.25. When $W_e \geq \sqrt{2\cot\beta/C} = 3.37$ (see [20]), a perfect-conductor film on a flat incline becomes unstable at $R = 0$; the topology of the neutral curves changes dramatically as W_e increases beyond 3.37 (see, for example, [27, Fig. 5]). For this reason, we do not consider higher values of the electric Weber number. It is worth noting that a perfect dielectric film becomes unstable at $R = 0$ when $W_e = 10.10$ for $\varepsilon = 3$, and when $W_e = 10.09$ for $\varepsilon = 0.5$ (see [20]).

The results in Fig. 4(a) show that in the absence of an electric field, when $W_e = 0$, the relative amplitude is a non-monotonic function of the Reynolds number. As R increases, it first grows to a maximum value before decreasing monotonically. The solid line in Fig. 4(a), corresponding to zero electric field strength, reaches a maximum at $R \approx 10.4$, which is beyond the critical Reynolds number for instability on a flat wall. As the inclination angle is reduced, a qualitatively similar curve to the solid line in Fig. 4(a) is found, but the maximum is larger and occurs at a higher Reynolds number which is always just beyond the critical value for stability on a flat wall. Interestingly, the overall effect of the electric field is to shift the amplitude curve down and to the left. In particular, the maximum

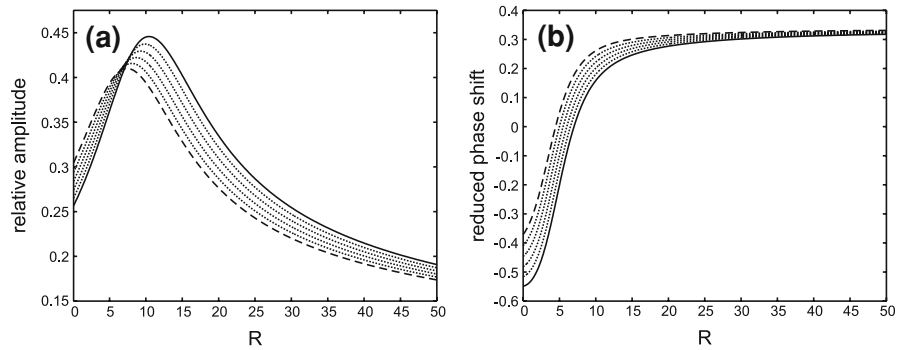

Fig. 5 The variation of (**a**) the relative amplitude, $|A_1|$, and (**b**) the reduced phase shift, $-\mathrm{Arg}(A_1)/(\pi/2)$, with the Reynolds number, R, for the case $C = 1$, $\beta = 10°$, and $k = 2$. The film is taken to be a perfect dielectric with $\varepsilon_p = 3$ and the different curves correspond to Weber numbers, W_e, that are evenly spaced from 0 (*solid line*) to 3.25 (*dashed line*)

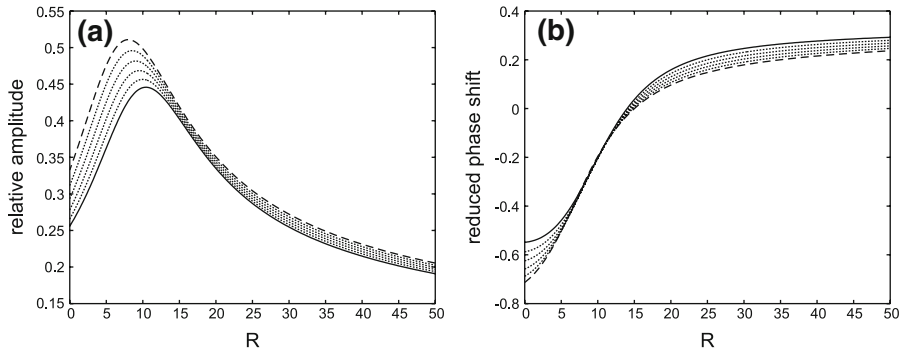

Fig. 6 The variation of (**a**) the relative amplitude, $|A_1|$, and (**b**) the reduced phase shift, $-\mathrm{Arg}(A_1)/(\pi/2)$, with the Reynolds number, R, for the case $C = 1$, $\beta = 10°$, and $k = 2$. The film is taken to be a perfect dielectric with $\varepsilon_p = 0.5$ and the different curves correspond to Weber numbers, W_e, that are evenly spaced from 0 (*solid line*) to 3.25 (*dashed line*)

shifts to a lower Reynolds number and into the stable regime for a flat film. The results in Fig. 4(b) indicate that the phase shift is a monotonically increasing function of the Reynolds number over the range of Weber numbers shown. The phase shift, which is negative at $R = 0$, increases with increasing R and vanishes at a critical value. At this point, the free surface is precisely in phase with the wall undulations. For a fixed value of R, the phase shift decreases monotonically as W_e increases. For the present parameter values, when R is less than about 14, it is possible to bring the surface wave into phase with the wall shape by introducing an electric field of sufficient intensity.

Results presented in Figs. 5(a, b) are for a perfect-dielectric film with $\varepsilon_p = 3$, so that the dielectric constant is larger in the film than above the film. The remaining parameter values are the same as for Fig. 4. The different curves correspond to evenly-spaced Weber numbers, W_e, between 0, shown as a solid line, and 3.25, shown as a dashed line. The results are qualitatively similar to the perfect-conductor case shown in Fig. 4. Again, the electric field lowers the maximum value of the relative amplitude and shifts it to a smaller Reynolds number. However, in this case the region of non-monotonic behaviour with varying W_e is sharply focused around $R \approx 7$. Figure 6(a, b) shows how the relative amplitude and the reduced phase shift respectively depend on the Reynolds number when $k = 2$ for a perfect-dielectric film with $\varepsilon_p = 0.5$, so that the dielectric constant is smaller in the film. The different curves correspond to evenly-spaced Weber numbers, W_e, between 0, shown as a solid line, and 3.25, shown as a dashed line. As might be expected, the results are qualitatively different to those found for a perfect-conductor and a perfect-dielectric film with $\varepsilon_p > 1$ discussed above. When R is fixed, the relative amplitude is a monotonically increasing function of W_e. The relative amplitude is notably less sensitive to changes in the electric field intensity at

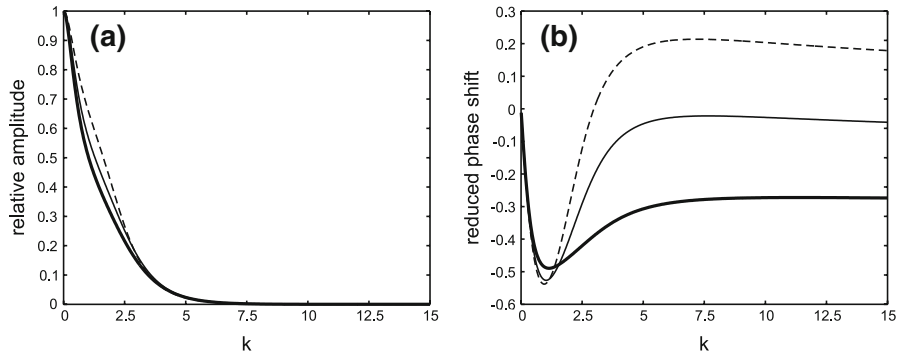

Fig. 7 The variation of (**a**) the relative amplitude, $|A_1|$, and (**b**) the reduced phase shift, $-\mathrm{Arg}(A_1)/(\pi/2)$, with the wavenumber, k, for the case $C = 1$, $W_e = 1$, $\beta = 10^\circ$. The film is taken to be a perfect conductor. The *thick solid*, *thin solid*, and *dashed lines* correspond to $R = 0$, $R = 2.5$ and $R = 5$ respectively

higher Reynolds number. In contrast to the previous cases, for small Reynolds number the phase shift decreases in magnitude when W_e increases, and the opposite situation obtains at higher Reynolds number. There is a significant range of the Reynolds number in between where the phase shift is comparatively insensitive to changes in the electric field intensity.

The relative amplitude tends to decrease when the wavenumber increases. At the same time, the phase shift first decreases and then tends to level out. This behaviour is evident in Fig. 7 where the relative amplitude, $|A_1|$, and reduced phase shift, $-\mathrm{Arg}(A_1)/(\pi/2)$, are plotted against wavenumber for the perfect-conductor model, with $\varepsilon_p = \infty$, for $R = 0,\ 2.5$, and 5. Regardless of the value of R, the relative amplitude approaches unity as k tends to zero and the phase shift tends to vanish, so that the surface waves are in phase with the wall corrugations. Conversely, as k increases, the relative amplitude decreases monotonically to zero and the free surface flattens out. Increasing the Reynolds number only has an appreciable effect over a range of wavenumbers between about 0 and 5. The Reynolds number has a much more substantial influence on the phase shift. In both the case of a perfect conductor and a perfect dielectric, in the presence of an electric field of sufficient strength, a sufficiently large increase in the Reynolds number will reduce the phase shift to zero and bring the surface waves into phase with the wall. Results for a perfect dielectric film with $\varepsilon_p = 3$ or $\varepsilon_p = 0.5$ and with the other parameter values kept the same are qualitatively similar to those presented in Fig. 7.

Bontozoglou and Papapolymerou [31] identified a resonance effect in viscous film flow similar to that discovered for the complementary problem for inviscid flow. At resonance, the relative amplitude of the surface wave is significantly larger than the amplitude of the wall corrugations, meaning in the present context that $|A_1|$ is significantly larger than unity. Bontozoglou and Papapolymerou [31] performed calculations in which the surface wave amplitude was found to be around 2.5 times the amplitude of the wall corrugations. Similar calculations were presented by Wierschem et al. [32], who provided evidence that the resonance is linked to an interaction between the falling film and gravity–capillary waves travelling in the opposite direction to the main flow. Experimental results which confirm the occurrence of static free surface waves in film flow over corrugated walls in the absence of an electric field have been reported by Argyriadi et al. [33]. To quantify the influence of an electric field on this inertial resonance, in Fig. 8(a) we display results for an electrified film acting as a perfect conductor for different values of W_e, where the other parameter values correspond to those selected by Wierschem et al. [32] to produce the $\delta = 1$ curve in their Fig. 2(a). Note that in the present notation Wierschem et al.'s pressure number is $P_{hc} = \cot\beta + 2C/k^2$, and their Reynolds number is 2/3 of ours. In line with the results presented above, the electric field lowers the maximum of the amplitude curve and thereby lessens the amplification effect at the point of resonance. Simultaneously, it shifts the maximum point to a lower Reynolds number. Similar qualitative features are apparent in Fig. 4(a), although here the amplitude of the surface wave at the maximum point is less than unity. When $W_e = 60$, the peak in the amplitude curve in Fig. 8(a) is almost completely ironed out, the amplitude of the surface wave is reduced to less than the amplitude of the wall corrugations, and the resonant amplification is removed. However, such a large value

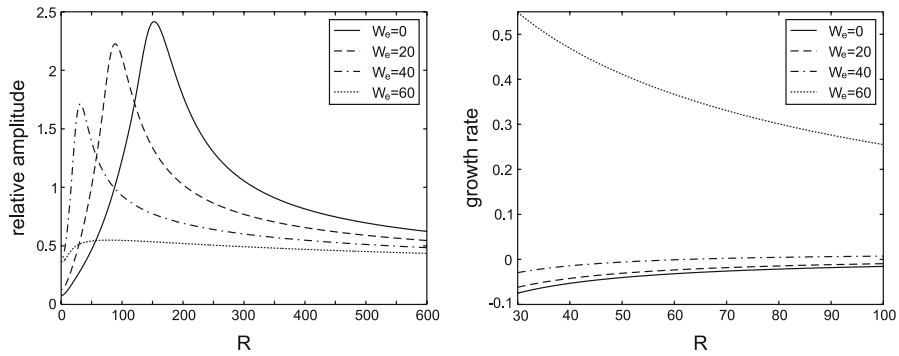

Fig. 8 (**a**) The relative amplitude, $|A_1|$, versus the Reynolds number, R, for the case $C = 0.01127936968$, $\beta = 10°$, and $k = 1$. The film is taken to be a perfect conductor. (**b**) The linear stability growth rate for the same parameter values as in (**a**)

of W_e may lie above the critical value for the surface disturbance forced by the wall profile to be stable. The stability graph in Fig. 8(b) shows the dominant growth rates computed from a normal mode linear stability analysis for a film flowing down an inclined flat wall (see, for example, Kim et al. [26] and Blyth [27]; the growth rates are defined precisely as in the latter paper). When the growth rate is positive, the film is unstable to perturbations with the same wavelength as the wall; when the growth rate is negative, the film is unstable to such perturbations. The growth rates are shown for a range of Reynolds numbers around the amplitude maxima in Fig. 8(a) over the same range of values of W_e. The amplitude maxima in Fig. 8(a) occur at $R = 141$ for $We = 0$, $R = 81$ for $We = 20$, and $R = 28$ for $We = 40$. In the last case, the maximal Reynolds number corresponds to a negative growth rate. We conclude that it does appear to be possible to use an electric field reduce the resonance effect to a significant degree before compromising the stability of the film.

4 Thin-film flow over a wall of finite amplitude

We now relax the assumption of small-amplitude corrugations and aim to derive a nonlinear equation for the film thickness $h \equiv f - s$, for an arbitrary choice of the wall shape, s. We work on the basis that streamwise variations in the film occur over a much larger lengthscale, λ, than the typical film thickness, h_0, so that the parameter $\delta \equiv h_0/\lambda$ is assumed to be small. Guided by the work of Tseluiko and Papageorgiou [21], we adopt scalings analogous to the case considered in Sect. 3.1.2 and write

$$C = \delta^2 \widetilde{C}, \quad W_e = \widetilde{W}_e/\delta, \tag{35}$$

where $\widetilde{C} = O(1)$ and $\widetilde{W}_e = O(1)$. Introducing the new independent variable $\xi = \delta x$ and proceeding as in Tseluiko and Papageorgiou [21], we derive an equation for the film thickness correct to $O(\delta^2)$,

$$\left[\frac{2}{3}h^3 + \frac{8}{15}\delta R h^6 h_\xi - \frac{2}{3}\delta \cot\beta h^3 (h+s)_\xi + \frac{\delta}{3\widetilde{C}} h^3 (h+s)_{\xi\xi\xi} + \frac{2}{3}\delta\left(1 - \frac{1}{\varepsilon_p}\right)\widetilde{W}_e h^3 \mathcal{H}\left[\left(1 - \frac{1}{\varepsilon_p}\right) h_{\xi\xi} + s_{\xi\xi}\right]\right]_\xi = 0, \tag{36}$$

where $\mathcal{H}$ denotes the Hilbert transform defined as

$$\mathcal{H}[g](\xi) = \frac{1}{\pi} PV \int_{-\infty}^{\infty} \frac{g(\xi')}{\xi - \xi'} \, \mathrm{d}\xi', \tag{37}$$

and PV denotes the principal value of the integral. Setting $s \equiv 0$ and taking the limit $\varepsilon_p \to \infty$ in (36), we recover the steady version of the long-wave evolution equation derived by Tseluiko and Papageorgiou [21] for the flow of a perfect-conductor film down an inclined plane.

We note that instead of (35) we might alternatively choose the scalings $C = O(\delta^3)$ and $W_e = O(\delta^{-2})$, similar to those considered in Sect. 3.1.1. Following through the analysis we derive an equation for the film thickness at leading order capturing both electrical and capillary effects, which reduces to the steady version of the equation obtained by Tseluiko et al. [22] in the limit $\varepsilon_p \to \infty$. Unfortunately, the Reynolds number does not appear in this equation and in order to bring in inertial effects we are forced to continue to $O(\delta^2)$ at least. The asymptotics quickly become extremely cumbersome and we do not pursue this here.

4.1 Results

For flow over a sinusoidal wall, we take

$$s(\xi) = a \sin(2\pi\xi/L), \tag{38}$$

where a is the amplitude and L is the wavelength. We compute numerical solutions to (36) using a finite-difference method similar to that described by Tseluiko et al. [22]. Choosing the small parameter $\delta = 0.2$, we solve (36) on the interval $-\pi \le \xi \le \pi$, which corresponds to the interval $-\pi/\delta \le x \le \pi/\delta$ for the unscaled variable $x = \xi/\delta$.

For general parameter values, increasing a from a small value up to 1 produces only a very small change in the free-surface shape. It remains virtually sinusoidal with almost the same phase shift relative to the wall. In Fig. 9, we show computed free-surface profiles for a wall of unit amplitude, $a = 1$, when $C' = 1$ and $\beta = 30°$. In each panel the solid lines correspond to $R = 0$, and the dashed lines correspond to $R = 10$. Figure 9(a) depicts film profiles when there is no electric field, $W_e' = 0$. When $R = 0$, the phase shift is small and negative. Raising the Reynolds number up to 10 produces a slight elevation in the amplitude of the free-surface deformation and a slight

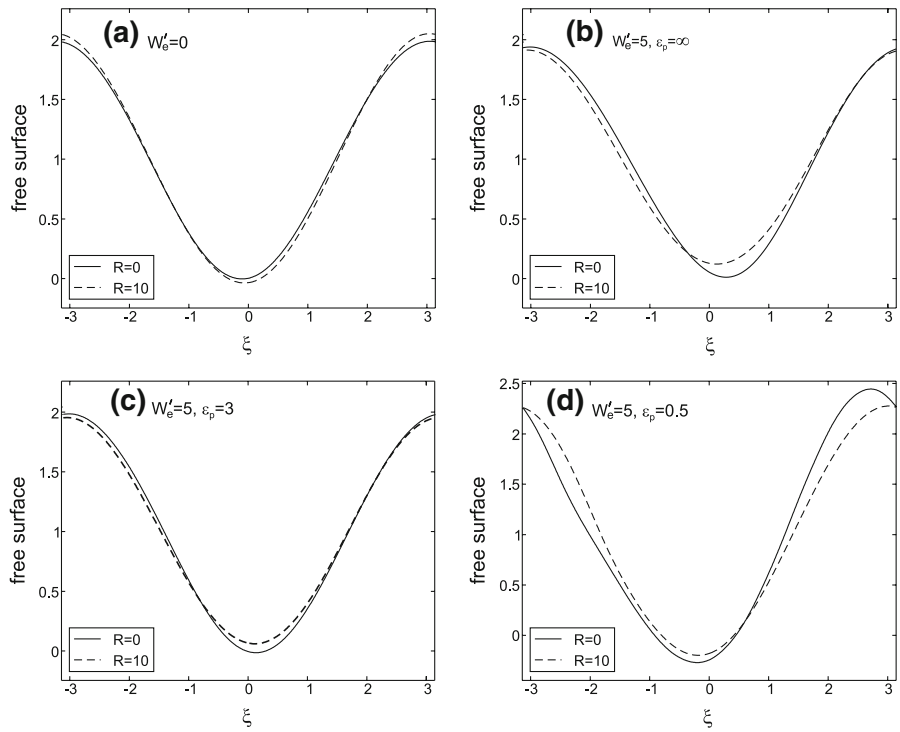

Fig. 9 The effect of the Reynolds number on the steady free-surface profile for a wall of unit amplitude, $s(\xi) = \sin(2\pi\xi/L)$ with $L = 2\pi$, when $C' = 1$ and $\beta = 30°$. Panel (**a**) corresponds to the case $W_e' = 0$, panel (**b**) corresponds to the case $W_e' = 5$ when the fluid is a perfect conductor, and panels (**c**) and (**d**) correspond to the case $W_e' = 5$ when the fluid is a perfect dielectric with $\varepsilon_p = 3$ and 0.5, respectively. The *solid lines* correspond to $R = 0$, and the *dashed lines* correspond to $R = 10$

increase in the phase shift, meaning that the free surface is moved to the right. For a perfect-conductor film with $W_e' = 5$ shown in Fig. 9(b), the free surface is again nearly sinusoidal. When $R = 0$, the phase shift is positive. Increasing the Reynolds number to 10 lowers the amplitude of the free-surface deformation and decreases the phase shift of the free surface. Similar results are found for a perfect-dielectric film with $\varepsilon_p = 3$ shown in Fig. 9(c) for the case $W_e' = 5$. In this case, raising the Reynolds number from 0 to 10 produces a smaller reduction in the amplitude and the phase shift compared to the perfect-conductor case. Fig. 9(d) displays the free-surface shape for a perfect-dielectric film with $\varepsilon_p = 0.5$ when $W_e' = 5$. The deviation of the free surface from a sinusoidal profile is more pronounced compared to the previous cases. When $R = 0$, the phase shift is small and negative. Increasing the Reynolds number to 10 reduces the amplitude and increases the phase shift, moving the free surface to the right. In conclusion, the mutual effect of the electric field and the Reynolds number on the free-surface shape is strongly dependent on the electrical properties of the film.

5 Discussion

We have examined the effect of inertia on the steady flow of a liquid film down a wavy wall in the presence of an electric field. In particular, we have studied how the surface characteristics of the film vary with Reynolds number under different assumptions for the electrical properties of the film. We considered both the case when the film is treated as a perfect conductor, when there is no electric field inside the liquid, and the case when the film is assumed to be a perfect dielectric supporting a potential difference between the wall and the free surface. Mathematically, the perfect conductor model is recovered in the limit when the relative permittivity between the film and the air tends to infinity. For perfect-dielectric films, we have considered both the case when the dielectric constant in the film is larger than in the air and vice versa.

Using perturbation analysis, we studied flow down a wall with small-amplitude sinusoidal corrugations, and derived a linearised disturbance equation and boundary conditions for the perturbed flow at arbitrary Reynolds number. Solutions were obtained numerically and compared with the results of a long-wave analysis based on the assumption of large wavelength corrugations. The results showed that for a perfector-conductor film the electric field either raises or lowers the amplitude of the surface disturbance depending on the prevailing Reynolds number. When the film behaves either as a perfect conductor or as a perfect dielectric with relative permittivity greater than one, the electric field tends to increase the phase shift between the surface deformation and the wall, regardless of the Reynolds number. When the Reynolds number lies below a threshold value, an electric field of the correct strength will bring the surface wave into phase with the wall profile. The results are markedly different when the relative permittivity is smaller than one. In this case, the electric field always raises the amplitude of the surface deformation irrespective of the size of the Reynolds number. Increasing the electric field strength reduces the phase shift between the surface wave and the wall except over a small range of Reynolds numbers where it has very little effect.

Relaxing the assumption of small-amplitude corrugations, we derived a nonlinear, non-local, long-wave equation for the film thickness and used it to study electrified film flow over a sinusoidal wall of finite amplitude. The perfect-conductor case and the perfect-dielectric case with $\varepsilon_p > 1$ are qualitatively similar, and both are qualitatively different to the perfect-dielectric case with $\varepsilon_p < 1$. For example, in the case studied, we found that when $\varepsilon_p > 1$, increasing the Reynolds number tends to decrease the phase shift between the free-surface profile and the wall. However, when $\varepsilon_p < 1$, increasing the Reynolds number tends to increase the phase shift.

In conclusion, inertia can have a mixed effect on the deformation and the phase shift of the free surface depending on the electrical properties of the fluid layer and the strength of the imposed electric field.

Acknowledgements This research was supported by the EPSRC under grant EP/D052289/1.

References

1. Stillwagon LE, Larson RG (1988) Fundamentals of topographic substrate leveling. J Appl Phys 63(11):5251–5258
2. Stillwagon LE, Larson RG (1990) Leveling of thin films over uneven substrates during spin coating. Phys Fluids A 2(11):1937–1944

3. Webb RL (1994) Principles of enhanced heat transfer. Wiley, New York
4. Karniadakis G, Beskok A, Aluru N (2005) Microflows and nanoflows: fundamentals and simulation. Springer, New York
5. Wang CY (1981) Liquid film flowing slowly down a wavy incline. AICh E J 27:207–212
6. Tougou H (1978) Long waves on a film flow of a viscous fluid down an inclined uneven wall. J Phys Soc Jpn 44:1014–1019
7. Wang CY (1984) Thin film flowing down a curved surface. J Appl Math Phys (ZAMP) 35(4):532–544
8. Wierschem A, Scholle M, Aksel N (2002) Comparison of different theoretical approaches to experiments on film flow down an inclined wavy wall. Exp Fluids 33:429–442
9. Pozrikidis C (1988) The flow of a liquid film along a periodic wall. J Fluid Mech 188:275–300
10. Wierschem A, Scholle M, Aksel N (2003) Vortices in film flow over strongly undulated bottom profiles at low Reynolds numbers. Phys Fluids 15:426–435
11. Scholle M, Wierschem A, Aksel N (2004) Creeping films with vortices over strongly undulated bottoms. Acta Mech 168:167–193
12. Wierschem A, Aksel N (2004) Influence of inertia on eddies created in films creeping over strongly undulated substrates. Phys Fluids 16(12):4566–4574
13. Malamataris NA, Bontozoglou V (1999) Computer aided analysis of viscous film flow along an inclined wavy wall. J Comput Phys 154:372–392
14. Trifonov YY (1999) Viscous liquid film flows over a periodic surface. Int J Multiph Flow 24(7):1139–1161
15. Gu F, Liu CJ, Yuan XG, Yu GC (2004) CFD simulation of liquid film flow on inclined plates. Chem Eng Technol 27(10):1099–1104
16. Luo H, Pozrikidis C (2006) Shear-driven and channel flow of a liquid film over a corrugated or indented wall. J Fluid Mech 556:167–188
17. Luo H, Blyth MG, Pozrikidis C (2008) Two-layer flow in a corrugated channel. J Eng Math 60:127–147
18. Gaskell PH, Jimack PK, Sellier M, Thompson HM, Wilson MCT (2004) Gravity-driven flow of continuous thin liquid films on non-porous substrates with topography. J Fluid Mech 509:253–280
19. Saprykin S, Koopmans RJ, Kalliadasis S (2007) Free-surface thin-film flows over topography: influence of inertia and viscoelasticity. J Fluid Mech 578:271–293
20. Tseluiko D, Blyth MG, Papageorgiou DT, Vanden-Broeck J-M (2008) Effect of an electric field on film flow down a corrugated wall at zero Reynolds number. Phys Fluids 20(4):042103
21. Tseluiko D, Papageorgiou DT (2006) Wave evolution on electrified falling films. J Fluid Mech 556:361–386
22. Tseluiko D, Blyth MG, Papageorgiou DT, Vanden-Broeck J-M (2008) Electrified viscous thin film flow over topography. J Fluid Mech 597:449–475
23. Melcher JR, Taylor GI (1969) Electrohydrodynamics: a review of the role of interfacial shear stresses. Annu Rev Fluid Mech 1:111–146
24. Jackson JD (1963) Classical electrodynamics. Wiley, New York
25. Yih C-H (1963) Stability of liquid flow down an inclined plane. Phys Fluids 6:321–334
26. Kim H, Bankoff SG, Miksis MJ (1992) The effect of an electrostatic field on film flow down an inclined plane. Phys Fluids A 4:2117–2130
27. Blyth MG (2007) Effect of an electric field on the stability of contaminated film flow down an inclined plane. J Fluid Mech 595:221–237
28. Vlachogiannis M, Bontozoglou V (2002) Experiments on laminar film flow along a periodic wall. J Fluid Mech 457:133–156
29. Wierschem A, Aksel N (2003) Instability of a liquid film flowing down an inclined wavy plane. Physica D 186:221–237
30. Wierschem A, Aksel N (2005) Effect of long undulated bottoms on thin gravity-driven films. Acta Mech 179:41–66
31. Bontozoglou V, Papapolymerou G (1997) Laminar film flow down a wavy incline. Int J Multiph Flow 23(1):69–79
32. Wierschem A, Bontozoglou V, Heining C, Uecker H, Aksel N (2008) Linear resonance in viscous films on inclined wavy planes. Int J Mulitph Flow 34:580–589
33. Argyriadi K, Vlachogiannis M, Bontozoglou V (2006) Experimental study of inclined film flow along periodic corrugations: the effect of wall steepness. Phys Fluids 18:012102